Research Article | Vol. 9, No. 7 / 1 July 2019 / Optical Materials Express 2748
Optical Materials EXPRESS

Pulse-induced transient blue absorption related with long-lived excitonic states in iron-doped lithium niobate

SIMON MESSERSCHMIDT, BJOERN BOURDON, DAVID BRINKMANN, ANDREAS KRAMPF, LAURA VITTADELLO, AND MIRCO IMLAU*

School of Physics, Osnabrueck University, Barbarastraße 7, 49076 Osnabrueck, Germany
**mirco.imlau@uni-osnabrueck.de*

Abstract: Transient absorption is studied in Fe-doped lithium niobate single crystals with the goal to control and probe a blue absorption feature related with excitonic states bound to Fe_{Li} defect centers. The exciton absorption is deduced from the comparison of ns-pump, supercontinuum-probe spectra obtained in crystals with different Fe-concentration and $Fe_{Li}^{2+/3+}$-ratio, at different pulse peak and photon energies as well as by signal separation taking well-known small polaron absorption bands into account. As a result, a broad-band absorption feature is deduced being characterized by an absorption cross-section of up to $\sigma^{max}(2.85\,eV) = (4 \pm 2) \cdot 10^{-22}\,m^2$. The band peaks at about 2.85 eV and can be reconstructed by the sum of two Gaussians centered at 2.2 eV (width ≈ 0.5 eV) and 2.9 eV (width ≈ 0.4 eV), respectively. The appropriate build-up and decay properties strongly depend on the crystals' composition as well as the incident pulse parameters. All findings are comprehensively analyzed and discussed within the model of $Fe_{Li}^{2+} - O^{-} - V_{Li}$ excitonic states.

1. Introduction

The microscopic understanding of pulse-induced transient absorption phenomena, such as green-induced infrared absorption (GRIIRA) [1] or blue-induced infrared absorption (BLIIRA) [2], is mandatory for the control of laser-induced damage mechanisms in lithium niobate ($LiNbO_3$, LN) and, thus, for applications of LN in nonlinear photonics [3]. From the beginning, the appearance of transient infrared absorption was successfully explained by the coupling of optically generated electrons with phonons, i.e., by the formation of $Nb_{Nb/Li}^{4+}$ small, strong-coupling electron polarons [4]. In contrast, the microscopic origin of transient blue-absorption remains fairly unexplained since advanced information about its respective features is still unsettled. In detail, neither the involved localized carrier states, nor their exact peak position, the shape, the band-width, and the absorption cross-section are known for the most of them. Furthermore, important knowledge to control the appearance of blue absorption by adjustment of, e.g., Fe-concentration, of the $Fe_{Li}^{2+/3+}$-ratio, and/or by means of pulse peak energy and/or photon energies is missing in literature completely, so far.

The presence of transient absorption in the blue-green spectral range in LN was discovered in 2005 by Herth *et al.* in Fe-doped LN using single probe-laser lines [5] and – as a first attempt – has been attributed to the coupling of optically generated holes with the lattice in direct vicinity of V_{Li} lithium vacancies. The formation of O^{-}-hole polarons with strong coupling is in full accordance with the original expectations formulated by Schirmer *et al.* for nearly all polar oxide crystals [6]. Later on, investigations with continuous wave [7] and pulsed laser light [8,9], however, revealed several discrepancies to the hole polaron model. The results of Waasem *et al.* [7] demanded for the existence of further electronic states within the band-gap, being handled

#363158 https://doi.org/10.1364/OME.9.002748
Journal © 2019 Received 22 Mar 2019; revised 8 May 2019; accepted 10 May 2019; published 3 Jun 2019

Optical Materials EXPRESS

as *X*-center of unknown microscopic nature. Quite recently, Messerschmidt *et al.* discussed excitonic states at the origin of long-lived transient blue absorption [9].

Self-trapped electron-hole-pairs at Nb-O-octahedra, commonly called *self-trapped excitons* (STEs) were widely investigated by Blasse *et al.* in nominally pure and doped LN by means of photoluminescence at temperatures below 100 K [10–12]. Similar luminescence phenomena were observed at room temperature using fs-NIR-pulse trains in Mg-doped LN [13] and have been assigned to the recombination of electron and hole polarons [14]. The goal of the work of Messerschmidt *et al.* [9] was to re-address charge-transport phenomena in LN by considering excitonic states as intermediate steps in addition. The authors succeeded to show, that the temperature dependence of transient absorption in LN crystals with Fe (and Mg) doping can be explained comprehensively by considering the presence of further (pinned) excitonic states, e.g., $Fe_{Li}^{2+} - O^{-} - V_{Li}$. It is noteworthy, that a main conclusion of this model approach is, that (pinned) STEs cause a pronounced long-lived blue absorption in Fe-doped LN (Fe:LN). We use the expression "pinned" in the context of this paper, if lattice defects or doping atoms hamper the movement and recombination of an STE in the regular lattice. In some cases, the pinned STE can be transformed into a self-trapped excitonic state in which at least one constituent is bound to the defect, e.g., the $Fe_{Li}^{2+} - O^{-} - V_{Li}$ STE.

In this paper, we address the open question about peak position, shape, bandwidth and absorption cross-section of the long-lived transient blue absorption under the assumption of self-trapped excitonic states as microscopic origin, i.e., following the general model approach of Ref. [9]. The study is performed using Fe-doped LN crystals according to previously reported pronounced transient blue absorption observed in these crystals. For the first time, ns-pump, supercontinuum-probe spectroscopy is applied in order to get a direct experimental access to the spectral shape of the optically induced excitonic blue absorption bands. At the same time, the determination of the temporal evolution of the absorption over a broad spectral range is mandatory for our analysis since it enables the spectral separation from further bound electronic states, such as, e.g., $Nb_{Li}^{4+/5+}$ or $Fe_{Li}^{2+/3+}$. These centers additionally show individual broad-band (≈ 1.0 eV) transient absorption [15] and, therefore, strongly overlap with the expected excitonic optical fingerprints. Quite recently, Schirmer *et al.* [16] and Sanson *et al.* [17] showed that the $Fe_{Li}^{2+/3+}$ center can be described in the small polaron model as well.

The experimental study is performed with LN crystals of various doping concentrations and $Fe_{Li}^{2+/3+}$-ratio in order to account for three of the most common optical excitation paths in Fe:LN [18–20]:

- Iron D-band excitation, $E_{abs}^{max} = 2.6$ eV: A charge transfer from iron to the conduction band: $Fe_{Li}^{2+} \rightarrow Nb_{Nb}^{5+}$
- Iron C-band excitation, $E_{abs} > 3.1$ eV: A charge transfer from the valence band to iron: $O^{2-} \rightarrow Fe_{Li}^{3+}$
- Interband excitation, $E_{abs} > (3.8 - 4.1)$ eV: A charge transfer from the valence to the conduction band: $O^{2-} \rightarrow Nb_{Nb}^{5+}$

Accordingly, photon energies at 2.33 eV (532 nm) and 3.49 eV (355 nm) are used to pump the transients.

The individual spectra reveal that any spectral and temporal feature of the $(E - t)$-plots can be modeled straightforwardly considering the additional presence of (pinned) excitonic states at iron. This knowledge is the anchor for the assignment of the excitonic absorption fingerprint from spectra obtained under rather different conditions. Finally, it is possible to analyze the main features (peak position, width) of the absorption band and, particularly to determine the respective absorption cross-section. For this purpose, the saturation of the $Fe_{Li}^{2+} - O^{-} - V_{Li}$ STE population is estimated by a pump intensity dependent measurement series. An instruction

Optical Materials EXPRESS

for the control of the transient blue absorption can be clearly deduced for Fe-doped LN. At the same time, the reconstruction of the excitonic absorption feature with probably two individual absorption bands demands for further investigations, in particular of the electronic transition mechanisms of excitonic states in LN.

2. Experimental methods

Our experimental series is performed by means of ns-pump, supercontinuum-probe absorption spectroscopy. Electronic detection at room temperature using continuous-wave, single line probe lasers at 2.54 eV (488 nm) and 1.58 eV (785 nm) are additionally applied as described in previous studies (cf. e.g. [9]). The combined setup is schematically depicted in Fig. 1. The supercontinuum setup obtains an accessible time range of 100 ns up to 100 s and is capable to detect carrier-lattice phenomena with strong coupling, whereas formation dynamics and intermediate trapping states, such as the intermediate trapping of small, free Nb^{4+}_{Nb} electron polarons, remain hidden.

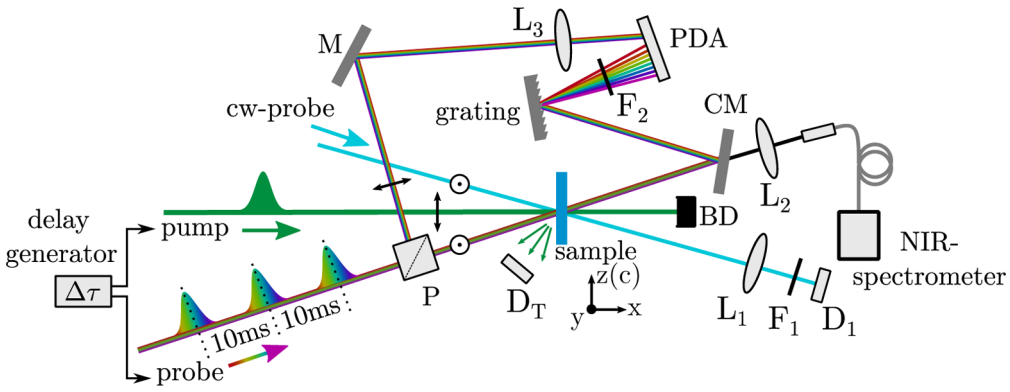

Fig. 1. Sketch of the ns-pump, supercontinuum-probe spectrometer applied in this study. The sample is pumped by a single pulse of a ns-pump pulse laser. Detection of the transient absorption is performed (i) using a diode (D_1) for the detection of the dynamic transmission change of a continuous wave probe laser transmitted through the sample (for a better visibility, only one cw-probe beam is shown) or (ii) by means of a supercontinuum. Here, the ns-pump pulse can be delayed for a certain time by a delay generator with respect to the supercontinuum probe pulse. The transmission change per wavelength is detected with two different spectrometers, one for the near-infrared part and one for the visible part of the supercontinuum pulse. $L_{1,2,3}$: lenses, $F_{1,2}$: optical filters, M: mirror, CM: cold mirror, P: polarizing beamsplitter cube, D_T: trigger diode for setup (i), BD: beam dump, PDA: photodiode array. The reader is referred to the text for further details.

A frequency-doubled and -tripled Nd:YAG pulse laser (Innolas Inc., *Spitlight*) and a broad-bandwidth light of a supercontinuum ns-pulse laser (LEUKOS, *STM-1-UV*) serve as pump (τ_{FWHM} = 8 ns, extraordinarily polarized, λ = 532 nm (2.33 eV) or λ = 355 nm (3.49 eV), respectively) and probe sources (τ_{FWHM} < 1 ns, unpolarized, λ = (350 – 1800) nm ≡ E = (3.54 – 0.69) eV, total average pulse energy of 35µJ). The probe pulse is split by a broadband polarizing beamsplitter cube into two parts with perpendicular polarization states, i.e., ordinary (transmitted) and extraordinary (reflected) with respect to the crystal's c-axis. The latter is used as a reference signal whereas the ordinary polarized part is adjusted to an optimum overlap with the pump within the sample's volume. After the sample, the probe light is split in a near-infrared (NIR) and visible (VIS) spectral region by a longpass dichroic mirror (λ_{cut} = 950 nm). A fiber-spectrometer (OceanOptics *NIRQuest 512*) and a discrete photodiode

Optical Materials EXPRESS

array (PDA, *Hamamatsu-S3902-512Q, TEC5*) are used simultaneously for the detection of the NIR and VIS signal fractions. A time resolution of up to 100 ns is achieved using an electronic delay of the pump. The time delay $\Delta\tau$ between pump and probe pulse is exponentially increased for t = 100 ns−10 ms so that the data points are equidistant on a logarithmic time axis. Data points for t> 10 ms are obtained by measuring the subsequent pulses of the supercontinuum laser taking advantage of its repetition rate of 100 Hz. The signal-to-noise ratio is increased by signal averaging over 20 individual measurements. The transient absorption is calculated from the transmitted intensities via $\alpha_{\mathrm{li}}(E,t) = -(1/d)\cdot\ln[I(E,t)/I(E,t\leq 0)]$, where $I(E,t)$ and $I(E,t\leq 0)$ are the transmitted probe light intensities after and before the pump pulse, respectively.

Our setup obeys minor limitations with respect to the spectral detection window, most of them being irrelevant for the purpose of our study: A lack of detection at 1.17 eV (1064 nm) and 2.33 eV (532 nm) due to a residual pump signal within the supercontinuum light and the SHG of the Nd:YAG pulse laser; one between 1.3 eV and 1.4 eV due to a low intensity of the supercontinuum laser and a weak sensitivity of the detectors; one above ≈ 3 eV due to a low intensity of the supercontinuum laser and a high intrinsic Fe_{Li}^{2+} steady-state absorption of Fe-doped LN (particularly visible in the data of section 3.1).

Four LN crystals of the congruently melting composition [21,22] with different Fe dopant concentrations in the melt were used as depicted in Table 1. All samples were cut in a manner that the crystallographic c-axis is parallel to the polished surface and the y-axis along one edge. The Fe_{Li}^{2+}-concentration ($c_{Fe_{Li}^{2+}}$) in the samples, obtained from MolTech GmbH (Fe:LN_1) and the University of Padova (Fe:LN_2, Fe:LN_3, and Fe:LN_4), was estimated by optical absorption measurements [23,24].

Table 1. Fe-doped LN crystals used in this study as obtained from MolTech GmbH (Fe:LN_1) and the University of Padova (Fe:LN_2, Fe:LN_3, and Fe:LN_4). The Fe_{Li}^{2+}-concentrations were determined by optical absorption measurements [23,24]. *d* is denoting the thickness of the sample and α(2.6 eV) the steady-state absorption at 2.6 eV.

Sample	d (mm)	α (2.6 eV) (m^{-1})	$c_{Fe_{Li}}$ (mol %)	$c_{Fe_{Li}^{2+}}$ ($10^{17}cm^{-3}$)	$c_{Fe_{Li}^{2+}}/c_{Fe_{Li}^{3+}}$
Fe:LN_1	2.0	468	0.185	10.4	0.029
Fe:LN_2	0.8	230	0.100	5.1	0.028
Fe:LN_3	2.0	45	0.020	1.0	0.027
Fe:LN_4	1.0	14	0.005	0.3	0.033

3. Experimental results

3.1. Excitation via the iron D-band

Figure 2 (left) shows the experimentally determined transient absorption for the case of optical excitation via the iron D-band, i.e., by means of a one-photon absorption process from Fe_{Li}^{2+} to Nb_{Nb}^{5+} (schematically sketched in Fig. 2 (right)).

The study is performed with sample Fe:LN_1 that obeys a high Fe_{Li}^{2+}-concentration. Furthermore, we have chosen a photon energy of 2.33 eV for the pump pulse that is close to resonant excitation (Fe_{Li}^{2+} peaks at 2.6 eV). The transients can be detected with sufficient signal-to-noise ratio in the spectral range of 0.7 eV to ≈ 3 eV and are exemplarily shown for a weak pulse peak intensity of $I_P \approx 30\,MW/cm^2$. The $(E-t)$-color plots are composed of two data sets that have been determined simultaneously with the VIS and NIR detector systems. The change of the light-induced absorption α_{li} is visualized by blue-yellow color coding as shown by the legend. Here, blue areas denote spectral regions with no change of the absorption upon the pump event, i.e., $\alpha_{\mathrm{li}} \approx 0\,m^{-1}$ and yellow regions mark noticeable changes with amplitudes up to $\alpha_{\mathrm{li}} = 75\,m^{-1}$. Black lines indicate a contour plot in steps of $\Delta\alpha_{\mathrm{li}} = 15\,m^{-1}$. Boxed white

Optical Materials EXPRESS

areas refer to the regions where spectral detection is not possible due to the above mentioned experimental limitations.

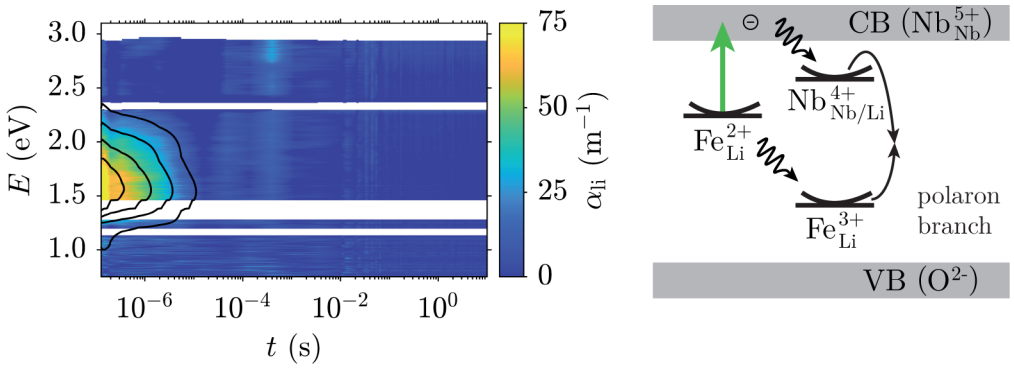

Fig. 2. Left: Transient absorption after an incident ns-pulse ($E = 2.33$ eV, $I_P \approx 30$ MW/cm^2) in the sample Fe:LN_1. The color coding of the light-induced absorption change is given in the legend on the right. Black lines indicate contour lines for steps of $\Delta\alpha_{li} = 15\,m^{-1}$. Boxed white areas refer to the regions where spectral detection is not possible. **Right:** Excitation and recombination scheme for the case of optical excitation via the iron D-band. For details see text.

This plot shows that a single, broad-band light-induced absorption feature is induced in the near-infrared immediately after the incident pump pulse. In more detail, it appears in the spectral window of $E = (0.7 - 2.5)$ eV with a peak at about 1.6 eV and shows a noticeable signal on the timescale up to 10μs. Within the experimental errors no change of the absorption shape during the decay can be observed. Further analysis of the spectra measured at $t = 100$ ns reveals a maximum value of $\alpha_{li}^{max} \approx 75\,m^{-1}$ with a full width at half maximum of ≈ 0.9 eV. In addition, the dynamic trace measured with a cw-laser at 1.58 eV can be reconstructed by means of a single stretched-exponential function [24] with a lifetime $\tau_{KWW}(1.58\,eV) = 10\,\mu s$ and stretching factor $\beta(1.58\,eV) = 0.4$.

3.2. *Excitation via the iron D-band + C-band*

Figure 3 (left) shows the experimentally obtained spectrum using conditions that additionally account for optical excitation via the C-band, i.e., via one-photon absorption from the O^{2-} valence band to Fe^{3+}_{Li} (cf. Fig. 3 (right)).

For this purpose, the sample Fe:LN_2 is used that was grown with a lower concentration of Fe in the melt. In addition, a photon energy of 3.49 eV of the pump pulse is used. Again, a moderate pump pulse intensity of $I_P \approx 27$ MW/cm^2 is chosen. The plot shows a considerable change of the transient absorption in comparison with the data of Fig. 2: a broad-band absorption feature appears immediately upon the incident pulse; it covers the total spectral range from the near-infrared to the blue, i.e., from 1.0 eV to 3.1 eV. A maximum of the light-induced absorption with values up to $\alpha_{li}^{max} \approx 350\,m^{-1}$ is determined. Along the time axis, a disappearance of the NIR signal within a few microseconds is obvious ($\tau_{KWW}(1.58\,eV) = 2\,\mu s$ and stretching factor $\beta(1.58\,eV) = 0.3$). In contrast, the long-lived blue absorption is nearly constant over tenth of milliseconds and develops a significant peak around 2.85 eV. It follows as well a single stretched-exponential function with $\tau_{KWW}(2.54\,eV) = 2$ s and $\beta(2.54\,eV) = 0.7$.

Optical Materials EXPRESS

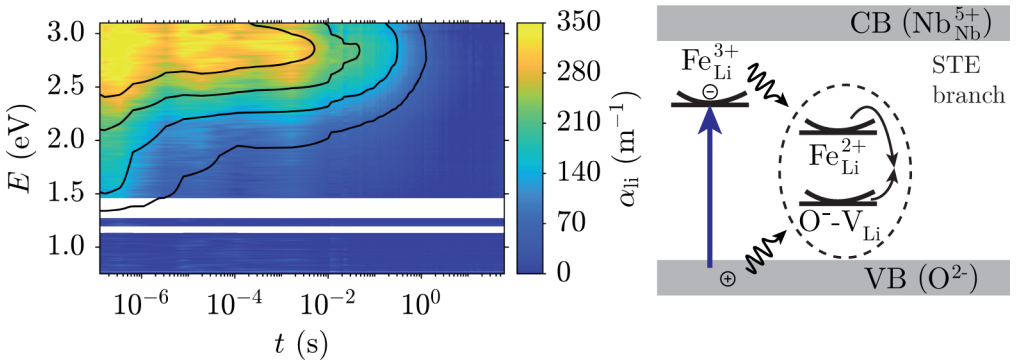

Fig. 3. Left: Transient absorption after an incident ns-pump pulse (E = 3.49 eV, $I_P \approx$ 27 MW/cm^2) in the sample Fe:LN_2. Color coding according to the legend on the right. The contour plot marks steps of $\Delta\alpha_{li}$ = 70 m^{-1}. Boxed white areas refer to the regions where spectral detection is not possible. **Right:** Excitation and recombination scheme for optical excitation via the iron C-band. For details see text.

3.3. *Excitation via the iron D-band + C-band + TPA*

Figure 4 (left) shows the results of our study using the sample Fe:LN_3, that features again a lower iron concentration in order to foster optical interband excitation, i.e., from the O^{2-} valence band to the Nb^{5+}_{Nb} conduction band (cf. Fig. 4 (right)).

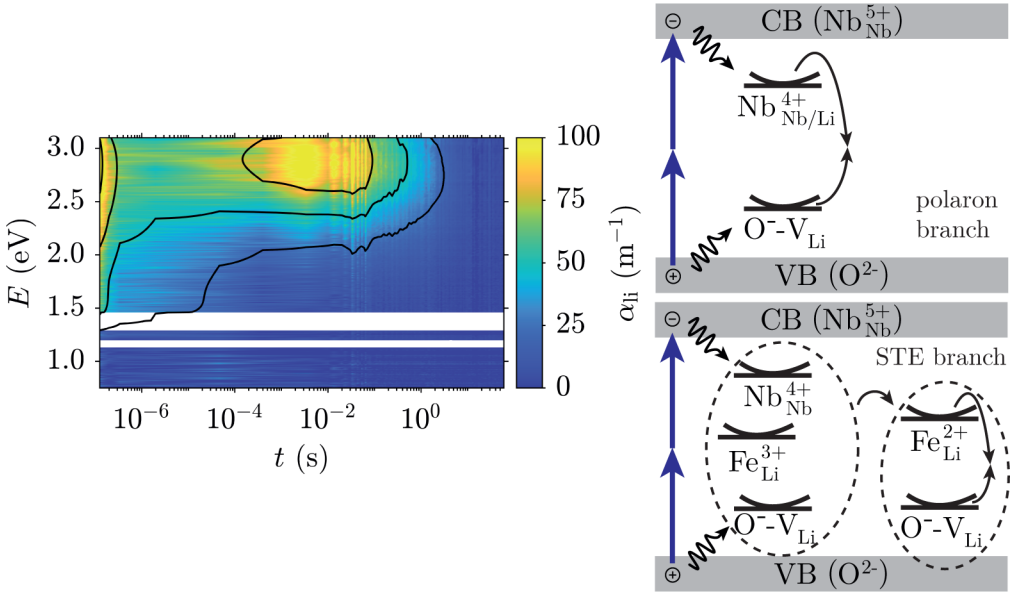

Fig. 4. Left: Supercontinuum transient absorption after 3.49 eV pulse exposure ($I_P \approx$ 12 MW/cm^2) in the sample Fe:LN_3 for the case of optical excitation via the D-band, C-Band and two-photon absorption. See legend on the right for color coding. The contour lines indicate steps of $\Delta\alpha_{li}$ = 25 m^{-1}. Boxed white areas refer to the regions where spectral detection is not possible. **Right:** Excitation and recombination scheme after excitation via a two-photon-absorption. For details see text.

Optical Materials EXPRESS

Again, a photon energy of 3.49 eV is chosen for the pump pulse with a comparably weak pulse peak intensity of $I_P \approx 12\,\mathrm{MW/cm^2}$. These experimental conditions result in the most complex dynamics of the transient absorption in Fe-doped LN: immediately upon the pump pulse, a broad-band absorption feature is detected with characteristics very similar to the situation in section 3.2, but with reduced maximum amplitude of the light-induced absorption with values up to $\alpha_{\mathrm{li}}^{\mathrm{max}} \approx 100\,\mathrm{m^{-1}}$. It is very remarkable that this initial absorption shows a fast decay all over the blue and NIR spectral range with nearly the same temporal behavior. It results in a complete decay of the signal in the NIR with $\tau_{\mathrm{KWW}}(1.58\,\mathrm{eV}) = 10\,\mu\mathrm{s}$ and $\beta(1.58\,\mathrm{eV}) = 0.3$. In contrast, a temporally constant transient absorption value ($\alpha_{\mathrm{li}} > 0\,\mathrm{m^{-1}}$) can be detected in the blue that remains over a duration of hundreds of microseconds. Subsequently, in the time range of milliseconds, the appearance of a delayed maximum with values up to $\alpha_{\mathrm{li}}^{\mathrm{max}} \approx 100\,\mathrm{m^{-1}}$ is detected. Similar to the findings in section 3.2, it peaks around 2.85 eV and the long decay can be described with the parameters $\tau_{\mathrm{KWW}}(2.54\,\mathrm{eV}) = 2\,\mathrm{s}$ and $\beta(2.54\,\mathrm{eV}) = 0.6$.

3.4. Absorption spectra and saturation of the long-lived blue absorption

Figure 5 shows the direct comparison of the long-lived transient blue absorption features as obtained from a more detailed analysis of the spectra depicted in Figs. 3 and 4.

The spectra were deduced by normalizing the data points at every delay position to the respective spectral maximum of the light-induced absorption and subsequently averaging the data set over the time interval from $t > 1 \cdot 10^{-3}\,\mathrm{s}$ to 10 s. Obviously, both spectra reveal a comparable shape with respect to the peak position of $E_{\mathrm{peak}} = (2.85 \pm 0.05)\,\mathrm{eV}$ and full width at half maximum of FWHM= $(1.00 \pm 0.25)\,\mathrm{eV}$.

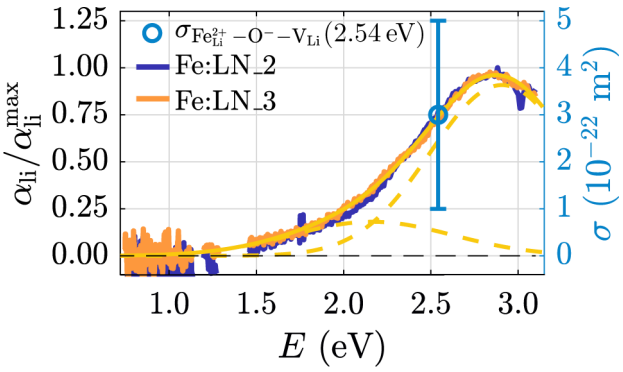

Fig. 5. Spectra of the long-lived blue absorption as deduced from the data in Fig. 3 and Fig. 4 by normalizing the data points at every delay position to the spectral maximum of the light-induced absorption and averaging the data set over the time interval from $t > 1 \cdot 10^{-3}$ s to 10 s. The yellow line represents a converging result of fitting Eq. (1) to the data. The dashed yellow lines refer to the individual Gaussians as given in Table 2. The blue data point is an experimentally determined value of the absorption cross-section at 2.54 eV and serves as scaling factor for the y-axis on the right.

Table 2. Parameters obtained from fitting the sum of two Gaussian functions (Eq. (1)) to the experimental data set for the case of two distinct absorption bands as sketched in Fig. 5. The fitting procedure reveals two solutions with a root mean square error of RMSE = 0.0387.

fit	a_1	a_2	b_1 (eV)	b_2 (eV)	c_1 (eV)	c_2 (eV)
1	0.91 ± 0.18	0.18 ± 0.17	2.91 ± 0.07	2.16 ± 0.50	0.41 ± 0.06	0.46 ± 0.17
2	0.37 ± 0.08	0.60 ± 0.40	2.88 ± 0.15	2.88 ± 0.34	0.31 ± 0.04	0.64 ± 0.03

Optical Materials EXPRESS

It is possible to reconstruct the absorption shape by the sum of two Gaussians via:

$$\frac{\alpha_{\mathrm{li}}(E)}{\alpha_{\mathrm{li}}^{\max}} = a_1 \cdot \exp\left[-\frac{(E-b_1)^2}{2c_1^2}\right] + a_2 \cdot \exp\left[-\frac{(E-b_2)^2}{2c_2^2}\right], \tag{1}$$

where $a_{1,2}$, $b_{1,2}$ and $c_{1,2}$ represent the amplitude, peak position and standard deviation of the individual Gaussian functions. As a result of the fitting procedure, two converging solutions are found. One, with two distinct absorption bands, is shown in Fig. 5. The associated fitting parameters are given in Table 2. A second converging solution of the fitting procedure results in two absorption bands peaking at the same photon energy of $E_{\mathrm{peak}} \approx 2.88\,\mathrm{eV}$, but with rather different amplitudes and FWHM values.

In order to check whether the long-lived blue absorption shows a saturation value at high intensities, we have performed appropriate measurements using our standard pump-probe experiment due to the higher signal-to-noise ratio and signal stability along with the use of a 2.54 eV continuous-wave laser system. Figure 6 shows the maximum amplitude $\alpha_{\mathrm{li}}^{\max}(2.54\,\mathrm{eV})$ measured for various pump intensities at $E_{\mathrm{P}} = 3.49\,\mathrm{eV}$ in the sample Fe:LN_4 which contains the lowest iron concentration in this study. The maximum amplitude follows at low pump intensities a quadratic behavior with increasing intensities. However, above $I_{\mathrm{P}} \approx 50\,\mathrm{MW/cm^2}$ the amplitudes start to saturate. The data can be described with the following function:

$$\alpha_{\mathrm{li}}^{\max}(E,I) = \alpha_{\mathrm{li}}^{\max}(E, I\to\infty) \cdot \left[1 - \exp\left(-\frac{I^2}{I_\alpha^2}\right)\right], \tag{2}$$

where $\alpha_{\mathrm{li}}^{\max}(E, I\to\infty)$ is the saturation value and I_α is the characteristic intensity. A fit of Eq. (2) to the data reveals $\alpha_{\mathrm{li}}^{\max}(2.54\,\mathrm{eV}, I\to\infty) = (276 \pm 25)\,\mathrm{m^{-1}}$ and $I_\alpha = (50 \pm 5)\,\mathrm{MW/cm^2}$.

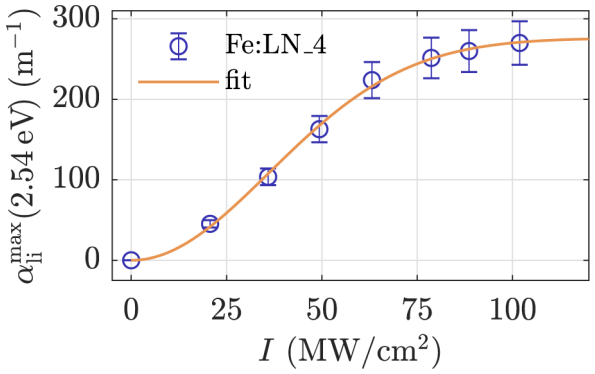

Fig. 6. Maximum amplitude of the long-lived blue absorption probed at 2.54 eV after pulse exposure at 3.49 eV for various intensities in the sample Fe:LN_4. The orange line is a fit of Eq. (2) to the data.

4. Discussion

Our experimental study reveals that ns-pump, supercontinuum-probe spectroscopy is successfully applied for the detection of transient absorption in Fe-doped lithium niobate. New insight to the temporal and, particularly, spectral evolution of pulse-induced absorption phenomena is obtained in the time interval from nanoseconds up to a few seconds and (nearly) without a gap from the blue to the near infrared spectral range. At a glance, the obtained $(E-t)$-plots demonstrate (i) the variety of transient absorption phenomena that appear in Fe-doped LN upon a single laser pulse, (ii) their complexity with respect to the spectral overlap of different absorption

Optical Materials EXPRESS

features as well as to a time-delayed build-up and (iii) their dependence on the experimental boundary conditions. The signal-to-noise-ratio is sufficient to resolve intensity changes in the order of $\delta I/I_0 \approx 0.5\,‰$. In this respect, the experimental detection by means of single-line continuous-wave laser beams remains as a mandatory tool for the detection of very weak signals and/or for the detailed inspection of the temporal shapes of the absorption features. The presented experimental combination brings together the advantage of both techniques and enables the comprehensive analysis of transient absorption in LN without any constraint.

In what follows, we will first discuss the individual data sets in more detail according to the state-of-the-art knowledge of small polarons with strong coupling and considering the model of (pinned) excitonic states, i.e., according to the previously reported model approach by Messerschmidt *et al.* [9]. Then, we focus on the absorption features of the $Fe_{Li}^{2+}-O^{-}-V_{Li}$ excitonic state and will deduce the respective absorption cross-section, peak position and bandwidth. It should be noted that we neglect the inclusion of the intrinsic luminescent $Nb_{Nb}^{4+} - O^{-}$ STE in all excitation/recombination schemes. It is because such centers are expected to appear predominantly in stoichiometric or Mg-doped LN in a time range much shorter than the used pulse duration, i.e., not accessible with our experimental setup (at room temperature) [9,25].

4.1. Excitation via the iron D-band

The experimental conditions resulting in the data presented in Fig. 2 (left) were prepared in a manner that a one-photon excitation via the iron D-band is highly preferred (high Fe_{Li}^{2+}-concentration, pump wavelength near the maximum of the Fe_{Li}^{2+} absorption band). We therefore analyze the transients by considering optical excitation/subsequent relaxation from/back to $Fe_{Li}^{2+/3+}$ and the interim formation of small $Nb_{Li/Nb}^{4+}$ polarons (c.f. Fig. 2 (right)). In particular, we expect that the pulse-induced absorption over the entire spectral range results from the interplay of a light-induced transparency due to less Fe_{Li}^{2+} (ground-state bleach) and an increased absorption due to the formation of small bound polarons, i.e., $\alpha_{li}(E) = \Delta N_{Nb_{Li}^{4+}} \cdot \sigma_{Nb_{Li}^{4+}}(E) + \Delta N_{Fe_{Li}^{2+}} \cdot \sigma_{Fe_{Li}^{2+}}(E)$. Here, $\Delta N_{Nb_{Li}^{4+}} = -\Delta N_{Fe_{Li}^{2+}}$ where ΔN is the change of concentration induced by the pump pulse. Considering the dispersion features of the two absorption species with well separated peak positions (1.6 eV and 2.6 eV) [15], a pronounced NIR absorption change shall remain that is mainly attributed to Nb_{Li}^{4+}. At the same time, no changes are expected for the blue-green spectral range since the absorption cross sections of Nb_{Li}^{4+} and Fe_{Li}^{2+} strongly overlap in this region and are nearly identical: $\sigma_{Fe_{Li}^{2+}}(\text{blue}) \approx \sigma_{Nb_{Li}^{4+}}(\text{blue})$ [15]. Our experimental findings in Fig. 2 are in full agreement with both expectations: a broad-band NIR absorption is clearly visible with nearly no absorption change in the blue-green spectral range (within the noise of our experiment). Moreover, three significant polaron fingerprints can be verified, particularly considering Nb_{Li}^{4+}: a lifetime in the sub-ms-time range, a NIR absorption feature with a peak at about 1.6 eV and a stretched-exponential decay behavior with a β-value below 1/2. We need to note, that in this discussion, we neglect the interim formation of Nb_{Nb}^{4+} free polarons due to experimental constraints: the free polaron lifetime is much shorter than the temporal resolution of our experiment [8]. A transient signal at the the peak maximum of small free polarons of about 1.0 eV [15] was therefore not observed. All these findings and interpretations are in full agreement with the state-of-the-art knowledge of the interaction of continuous-wave and pulsed laser light with Fe-doped LN at moderate average power [24,26].

4.2. Excitation via the iron D-band + C-band

The second measurement was performed with an iron-doped LN sample containing a lower Fe-concentration and with a pump wavelength in the UV. This fosters the optical excitation via the iron C-band, though an excitation via the D-band cannot be excluded. We additionally need to consider that the cross-sections of these two excitation paths are very similar at 355 nm [27],

Optical Materials EXPRESS

i.e, a contribution of both paths to the transient spectrum is to be expected. In this sense, and in direct comparison with the discussion of the previous section, it is likely to assume that the observed NIR absorption feature with fast decay in the spectra of Fig. 3 originates from the mechanisms associated with the D-band excitation (see section 4.1). All deduced experimental features (peak position, lifetime, stretching factor) support this assumption. Accordingly, the UV-induced long-lived blue absorption in Fig. 3 is assigned to the second excitation path via the iron C-band. To the best of our knowledge, the latter has not been investigated in the context of either small polarons or STEs in lithium niobate, so far. At a first glance, a relation to the formation of small $O^- - V_{Li}$ hole and Fe_{Li}^{2+} polarons may be assumed considering the charge-transfer from O^{2-} to Fe_{Li}^{3+} [18] (c.f. Fig. 3 (right)). However, in this case, the blue absorption must feature a broad-band absorption centered in the range of 2.5 – 2.6 eV [6,15], that does not correspond with the experimentally determined peak position of about 2.85 eV in our spectra (see Fig. 5 and discussion below). An alternative microscopic approach is to consider $Fe_{Li}^{2+} - O^- - V_{Li}$ STEs as proposed by Messerschmidt *et al.* [9]. Such states are reported to form after pinning and subsequent transformation of an intrinsic STE at an iron center within a few hundred microseconds. They show absorption in the blue-green spectral range and their decay dynamics feature a stretching factor $\beta > 2/3$. According to the characteristics of the induced blue absorption deduced from the data in Fig. 2 (absorption feature with a peak at about 2.85 eV, an increased stretching factor of $\beta \approx 0.7$), it is reasonable to assume the presence of such states in our case, as well. A remarkable consequence of this approach is that the direct STE formation via the C-band is discovered for the first time. This finding is of particular importance of applications with doped LN and ultraviolet laser pulses, e.g., UV photorefraction.

4.3. Excitation via the iron D-band + C-band + TPA

The third measurement in this study was performed with a sample containing a lower Fe_{Li}^{2+}- and Fe_{Li}^{3+}-concentration and, thus, also obeys the one-photon excitation and the subsequent recombination paths via the iron C- and D-band as discussed in the two previous sections 4.1 and 4.2. In addition, the low Fe-concentration increases the probability for excitation via two-photon absorption (TPA). It is because the negligible fundamental absorption conserves the peak intensity of the incident laser pulse. The influence of the electron-hole-pairs generated via TPA on the decay dynamics can be deduced by comparing the results in the two previous sections 4.1 and 4.2 with the data in section 3.3 (c.f. Fig. 4). The main differences are (i) an additional fast decay and (ii) a delayed increase in the blue spectral range. Both phenomena can be explained as follows: the generation of electron-hole pairs in the LN-host lattice results in the formation of $O^- - V_{Li}$ hole and Nb_{Li}^{4+} bound polarons as well as STEs which can be pinned next to Fe_{Li}^{3+} (c.f. Fig. 4 (right)). The formed polarons/STEs contribute to the transient spectra with absorption features in the blue and near-infrared spectral range. The decay of the initial transient signals in the blue and NIR spectral range is a characteristic fingerprint for the recombination of hole polarons with bound polarons known from undoped lithium niobate samples [3,15]. However, in contrast to an undoped sample, the initial temporal decay in the blue spectral range is superimposed by the transformation of pinned STEs at Fe_{Li}^{3+} into $Fe_{Li}^{2+} - O^- - V_{Li}$ inducing a strong blue absorption in the time range of milliseconds [9]. The observed complex behavior in the blue spectral range then is due to the different decay dynamics of the hole/bound polaron recombination on the one hand and the transformation of pinned STEs on the other hand.

4.4. Determination of the shape and absorption cross-section of the long-lived blue absorption

The discussion of the previous sections points to a dominant role of $Fe_{Li}^{2+} - O^- - V_{Li}$ STEs at the origin of the long-lived blue absorption in Fe-doped LN which is in accordance with Ref. [9]. Following this microscopic approach, the spectra of Fig. 3 and Fig. 4 will both be related with

Optical Materials EXPRESS

this excitonic state. Figure 5 compares the spectral shapes of the long-lived blue absorption as obtained from a further analysis of these data sets. Obviously, both spectra are characterized by a comparable shape, peak position and bandwidth and are nearly indistinguishable from each other. This result is very remarkable since the data sets were obtained in two completely different Fe-doped LN crystals and by using different pulse intensities for excitation. Moreover, it supports the finding that $Fe_{Li}^{2+} - O^{-} - V_{Li}$ STEs can be formed directly after the pump pulse via the iron C-band.

Let us now further analyze the absorption spectrum depicted in Fig. 5 in the microscopic model of $Fe_{Li}^{2+} - O^{-} - V_{Li}$ STEs. First, we discuss the shape of the STE absorption feature. Figure 5 shows that the pulse-induced absorption appears with a large amplitude over the entire VIS-NIR spectral region that is experimentally accessible with our setup. It can be expected that the band extends even far into the ultraviolet region and, that it overlaps with the interband absorption (starting at about 3.8 eV). Fitting the spectrum in the accessible region reveals that at least the sum of two Gaussian functions (c.f. Eq. (1)) with six free fitting parameters is required for its description. Exemplarily, one of the converging solutions is depicted in Fig. 5 with different peak positions (2.2 eV and 2.8 eV, respectively) but comparable FWHMs of the constituents (c.f. Table 2). We note that it is alternatively possible to perform the fitting procedure with two Gaussians at the same peak position (of about 2.9 eV), but with different FWHM values.

Taking these findings into account, we refer to the state-of-the-art knowledge of STE absorption bands and find that they typically resemble the interplay of at least two spectrally separated single bands in a first approximation [28–30]: a straightforward explanation is that the two bands originate from an optical excitation of both the electron and the hole to higher states, respectively. Or, the two bands refer to the photo-ionization process of STEs. Against this background, it is reasonable to expect two absorption bands for STEs in LN as well, one associated with the electron excitation from Fe_{Li}^{2+} and the other one from the $O^{-} - V_{Li}$-center. Peak position, bandwidth and the relative fraction of the total absorption amplitude (c.f. Table 2) then reflect the individual absorption features and absorption cross-sections of the two constituents involved. In particular, the effective absorption coefficient of the STE then is given by $\alpha_{\mathrm{eff}}(E) = \alpha_1(E) + \alpha_2(E)$ in this case.

Second, we intend to estimate the effective absorption cross-section of the $Fe_{Li}^{2+} - O^{-} - V_{Li}$ STE. For this purpose, following the discussion of the previous paragraph, it is assumed that the absorption feature originates from a single absorption center of number density N, i.e., $\alpha_{\mathrm{eff}}(E) = \sigma_{\mathrm{eff}}(E) \cdot N$. In our case, the number density N can be determined experimentally by intensity dependent measurements of $\alpha_{\mathrm{li}}(I)$ as depicted in Fig. 6. It is because $N(I)$ saturates due to a limited Fe_{Li}^{3+}-concentration such that $\alpha_{\mathrm{li}}(I)$ saturates, too. The experimentally determined saturation value $\alpha_{\mathrm{li}}^{\mathrm{max}}(E, I \to \infty)$ then enables the calculation of the effective cross-section via $\sigma_{\mathrm{eff}}(E) = \alpha_{\mathrm{li}}^{\mathrm{max}}(E, I \to \infty)/c_{Fe_{Li}^{3+}}$. This study has been performed at a minimum total iron concentration to (i) ensure that a saturation value can be achieved with our experimental conditions and (ii) enable the utilization of low pump intensities to avoid laser induced damages. With the data deduced from Fig. 6 we obtain $\sigma_{\mathrm{eff}}(2.54\,\mathrm{eV}) = (3 \pm 2) \cdot 10^{-22}\,\mathrm{m}^2$. This value serves for scaling the right y-axis in Fig. 5 which leads to a maximum effective cross-section of $\sigma_{\mathrm{eff}}^{\mathrm{max}}(2.85\,\mathrm{eV}) = (4 \pm 2) \cdot 10^{-22}\,\mathrm{m}^2$. The large error of these values is a combination of both, the precision of our measurement and the determination of the iron concentration. We would also like to mention that the estimated values are only a lower bound because the calculation is based on the assumption that all Fe_{Li}^{3+}-centers are occupied in the saturation state. If this assumption is inapplicable, the number density of STEs is reduced which will result in a larger value of the absorption cross-section. In comparison to small polarons in lithium niobate [15], the absorption cross-section of the STE is in the same order of magnitude. Assuming that (pinned) STEs formed under similar conditions, e.g., in Mg-doped LN, exhibit similar absorption bands and

Optical Materials EXPRESS

cross-sections, they have to play an important role in the blue absorption and might be responsible for a damping of frequency conversion and laser induced damages in this spectral range.

5. Conclusion

This study reveals the striking impact of ns-pump, supercontinuum-probe spectroscopy for the microscopic understanding of strongly localized electronic states in oxide crystals with lithium niobate as an example. The spectra allow to distinguish the temporal and spectral action of individual optically generated species under rather different experimental conditions and their formation/transport/recombination/relaxation description within a quite complex band model scheme. As a result it is possible to discover new properties of the interaction of light pulses with a strong polar crystal, e.g., the possibility to optically generate $Fe_{Li}^{2+} - O^{-} - V_{Li}$ STEs directly by a charge transfer via the iron C-band. Furthermore, the STE absorption cross-section obeys similar values as reported for small polarons. Another impressive result of this study is that the combination of transient spectroscopy and the polaron/exciton model in LN enables the precise prediction of the complex dynamics of transient absorption over a large spectral and temporal range. At the same time, it supports the validity of the model of (pinned) STEs for lithium niobate, which have been disregarded in the mechanisms of light-induced transport, so far. Our findings are of particular importance for the field of photorefraction since the formation of STEs will not result in the optically induced separation of charges that is mandatory for the photorefractive effect. The possibility to solely generate excitonic states by means of optical adjustment of pulse parameters (photon energy, pulse peak energy) and/or material adjustment ($Fe^{2+/3+}$-ratio) enables, e.g., the efficient suppression of optical damage in LN-based frequency converters. In the same manner, it is possible to determine temporal regimes that allow for photorefractive recording at elevated efficiencies, such as, e.g., the sub-millisecond time range for recording with a single, intense laser pulse.

Funding

Deutscher Akademischer Austauschdienst (DAAD) (57390412); Deutsche Forschungsgemeinschaft (DFG) (IM37/11-1, INST 190/165-1 FUGG); Osnabrueck University (Open Access Fund).

Acknowledgements

The authors are indebted to thank Marco Bazzan and coworkers for crystals and crystal preparation as well as Christoph Merschjann for fruitful discussion.

References

1. R. Batchko, G. Miller, A. Alexandrovski, M. Fejer, and R. Byer, "Limitations of high-power visible wavelength periodically poled lithium niobate devices due to green-induced infrared absorption and thermal lensing," Tech. Dig. Summ. Pap. Present. at Conf. on Lasers Electro-Optics. Conf. Ed. 1998 Tech. Dig. Series, Vol. 6 (IEEE Cat. No.98CH36178) (1998).
2. H. M. Yochum, K. B. Üçer, R. T. Williams, L. Grigorjeva, D. Millers, and G. Corradi, "Subpicosecond Laser Spectroscopy of Blue-Light-Induced Absorption in $KNbO_3$ and $LiNbO_3$," Defects Surface-Induced Eff. Adv. Perovskites pp. 125–138 (2000).
3. M. Imlau, H. Badorreck, and C. Merschjann, "Optical nonlinearities of small polarons in lithium niobate," Appl. Phys. Rev. **2**(4), 040606 (2015).
4. Y. Furukawa, K. Kitamura, A. Alexandrovski, R. K. Route, M. M. Fejer, and G. Foulon, "Green-induced infrared absorption in MgO doped $LiNbO_3$," Appl. Phys. Lett. **78**(14), 1970–1972 (2001).
5. P. Herth, T. Granzow, D. Schaniel, T. Woike, M. Imlau, and E. Krätzig, "Evidence for Light-Induced Hole Polarons in $LiNbO_3$," Phys. Rev. Lett. **95**(6), 067404 (2005).
6. O. F. Schirmer, "O^{-} bound small polarons in oxide materials," J. Phys.: Condens. Matter **18**(43), R667–R704 (2006).
7. N. Waasem, A. Markosyan, M. M. Fejer, and K. Buse, "Green-induced blue absorption in MgO-doped lithium niobate crystals," Opt. Lett. **38**(16), 2953 (2013).

Optical Materials EXPRESS

8. D. Conradi, C. Merschjann, B. Schoke, M. Imlau, G. Corradi, and K. Polgár, "Influence of Mg doping on the behaviour of polaronic light-induced absorption in $LiNbO_3$," Phys. Status Solidi RRL **2**(6), 284–286 (2008).
9. S. Messerschmidt, A. Krampf, F. Freytag, M. Imlau, L. Vittadello, M. Bazzan, and G. Corradi, "The role of self-trapped excitons in polaronic recombination processes in lithium niobate," J. Phys.: Condens. Matter **31**(6), 065701 (2019).
10. D. M. Krol, G. Blasse, and R. C. Powell, "The influence of the Li/Nb ratio on the luminescence properties of $LiNbO_3$," J. Chem. Phys. **73**(1), 163–166 (1980).
11. M. Wiegel, M. Emond, E. Stobbe, and G. Blasse, "Luminescence of alkali tantalates and niobates," J. Phys. Chem. Solids **55**(8), 773–778 (1994).
12. M. Wiegel, G. Blasse, A. Navrotsky, A. Mehta, N. Kumada, and N. Kinomura, "Luminescence of the Ilmenite Phase of $LiNbO_3$," J. Solid State Chem. **109**(2), 413–415 (1994).
13. P. Reichenbach, T. Kämpfe, A. Haußmann, A. Thiessen, T. Woike, R. Steudtner, L. Kocsor, Z. Szaller, L. Kovács, and L. Eng, "Polaron-Mediated Luminescence in Lithium Niobate and Lithium Tantalate and Its Domain Contrast," Crystals **8**(5), 214 (2018).
14. T. Kämpfe, A. Haußmann, L. M. Eng, P. Reichenbach, A. Thiessen, T. Woike, and R. Steudtner, "Time-resolved photoluminescence spectroscopy of Nb_{Nb}^{4+} and O^- polarons in $LiNbO_3$ single crystals," Phys. Rev. B **93**(17), 174116 (2016).
15. C. Merschjann, B. Schoke, D. Conradi, M. Imlau, G. Corradi, and K. Polgár, "Absorption cross sections and number densities of electron and hole polarons in congruently melting $LiNbO_3$," J. Phys.: Condens. Matter **21**(1), 015906 (2009).
16. O. F. Schirmer, M. Imlau, and C. Merschjann, "Bulk photovoltaic effect of $LiNbO_3$:Fe and its small-polaron-based microscopic interpretation," Phys. Rev. B **83**(16), 165106 (2011).
17. A. Sanson, A. Zaltron, N. Argiolas, C. Sada, M. Bazzan, W. G. Schmidt, and S. Sanna, "Polaronic deformation at the $Fe^{2+/3+}$ impurity site in Fe:$LiNbO_3$ crystals," Phys. Rev. B **91**(9), 094109 (2015).
18. M. G. Clark, F. J. DiSalvo, A. M. Glass, and G. E. Peterson, "Electronic structure and optical index damage of iron-doped lithium niobate," J. Chem. Phys. **59**(12), 6209–6219 (1973).
19. B. Dischler, J. Herrington, A. Räuber, and H. Kurz, "Correlation of the photorefractive sensitivity in doped $LiNbO_3$ with chemically induced changes in the optical absorption spectra," Solid State Commun. **14**(11), 1233–1236 (1974).
20. L. Kovács, G. Ruschhaupt, K. Polgár, G. Corradi, and M. Wöhlecke, "Composition dependence of the ultraviolet absorption edge in lithium niobate," Appl. Phys. Lett. **70**(21), 2801–2803 (1997).
21. J. R. Carruthers, G. E. Peterson, M. Grasso, and P. M. Bridenbaugh, "Nonstoichiometry and Crystal Growth of Lithium Niobate," J. Appl. Phys. **42**(5), 1846–1851 (1971).
22. T. Volk and M. Wöhlecke, *Lithium Niobate: Defects, Photorefraction and Ferroelectric Switching*, Springer Series in Materials Science (Springer Berlin Heidelberg, 2008).
23. H. Kurz, E. Krätzig, W. Keune, H. Engelmann, U. Gonser, B. Dischler, and A. Räuber, "Photorefractive centers in $LiNbO_3$, studied by optical-, Mössbauer- and EPR-methods," Appl. Phys. **12**(4), 355–368 (1977).
24. D. Berben, K. Buse, S. Wevering, P. Herth, M. Imlau, and T. Woike, "Lifetime of small polarons in iron-doped lithium–niobate crystals," J. Appl. Phys. **87**(3), 1034–1041 (2000).
25. F. Klose, M. Wöhlecke, and S. Kapphan, "UV-excited luminescence of $LiNbO_3$ and $LiNbO_3$:Mg," Ferroelectrics **92**(1), 181–187 (1989).
26. P. Herth, D. Schaniel, T. Woike, T. Granzow, M. Imlau, and E. Krätzig, "Polarons generated by laser pulses in doped $LiNbO_3$," Phys. Rev. B **71**(12), 125128 (2005).
27. M. V. Ciampolillo, A. Zaltron, M. Bazzan, N. Argiolas, and C. Sada, "Quantification of Iron (Fe) in Lithium Niobate by Optical Absorption," Appl. Spectrosc. **65**(2), 216–220 (2011).
28. R. T. Williams and M. N. Kabler, "Excited-state absorption spectroscopy of self-trapped excitons in alkali halides," Phys. Rev. B **9**(4), 1897–1907 (1974).
29. R. Williams and K. Song, "The self-trapped exciton," J. Phys. Chem. Solids **51**(7), 679–716 (1990).
30. P. Li, S. Gridin, K. B. Ucer, R. T. Williams, and P. R. Menge, "Picosecond absorption spectroscopy of self-trapped excitons and transient Ce states in $LaBr_3$ and $LaBr_3$:Ce," Phys. Rev. B **97**(14), 144303 (2018).